Available online at www.sciencedirect.com
SCIENCE DIRECT®
Journal of Photochemistry and Photobiology A: Chemistry 162 (2004) 339–351
Journal of Photochemistry and Photobiology A:Chemistry
www.elsevier.com/locate/jphotochem

Photoinitiation of buthylmethacrylate polymerization by colloidal semiconductor nanoparticles

A.L. Stroyuk*, V.M. Granchak, A.V. Korzhak, S.Ya. Kuchmii

[a] *Photochemistry Department, L.V. Pysarzhevsky Institute of Physical Chemistry, National Academy of Sciences of Ukraine, 31 Prosp. Nauky, Kyiv 03028, Ukraine*

Received 23 July 2003; received in revised form 28 August 2003; accepted 28 August 2003

Abstract

Nanoparticles of zinc and iron oxides as well as cadmium sulfide of different size were synthesized in 2-propanol, their band gaps and allowed bands positions were determined. The foregoing nanoparticles turned out to be efficient photoinitiators of butylmethacrylate polymerization. On the basis of the kinetic parameters of the process a free radical mechanism of the butylmethacrylate photopolymerization induced by investigated nanosized semiconductors was inferred. An increase in the specific rate of the butylmethacrylate photopolymerization with the decrease in the average CdS nanoparticles diameter was explained in terms of the theory of quantum confinement effects in semiconductors and was attributed to an increase in the probability of monomer reduction by photogenerated electrons of CdS nanocrystals conduction band with the diminishing of crystals size.

It was shown that a number of xanthene dyes—fluorescein and its halogenated derivatives are efficient sensitizers of ZnO nanoparticles to the visible light. Butylmethacrylate photopolymerization rates grow at the presence of ZnO nanoparticles and sensitizers symbately with an increase in singlet and triplet-excited states energy of dyes studied. Such relation indicates the determining role of the process of electron transfer from photoexcited sensitizers to the ZnO nanoparticles conduction band in the initiation stage of polymerization. Flash photolysis was used for the investigation of the nature and decay characteristics of short-lived intermediates generated in systems consisting of ZnO nanoparticles, sensitizers and monomer. Schemes of the mechanism of the butylmethacrylate photopolymerization induced by investigated nanosized semiconductors were proposed.

Keywords: Photopolymerization; Semiconductor nanoparticles; Cadmium sulfide; Zinc oxide; Iron oxide; Sensitization

1. Introduction

Photopolymerization compositions find applications for various manufacturing processes including production of printing stencils, photoresists, photocurable varnishes and paints, holographic and optical materials for electronic and instrument-making industry, etc. [1]. Various organic compounds [1,2], transition metals complexes [2], semiconductor suspensions and electrodes [3–7] are widely used as light-sensitive components for such compositions. Photopolymerization of various monomers can be also initiated by ultrasmall semiconductor particles [8–10]. Such photoinitiators attract considerable attention due to their intrinsical negligibly small light scattering, great specific surface area, manifestation of quantum confinement effects, etc. [11,12]. Furthermore, utilization of semiconductor nanoparticles not only as polymerization photoinitiators, but at the same time as superfine polymer fillers offers new ways to novel promising composit materials composed of organic polymers and inorganic high-dispersed semiconductors [13,14].

The paper represents the results of the investigation of buthylmethacrylate (BMA) polymerization in 2-propanol induced by light-excited nanometer colloidal particles of cadmium sulfide, iron(III) and zinc oxides. Relationships between photopolymerization rates and semiconductor nature, light intensity, size and concentration of semiconductor particles were determined, the possibility of sensitization of photopolymerization compositions containing nanometer zinc oxide particles with some xanthene dyes—fluorescein (F) and its halogenated derivatives was established. Taking into account that both monomer and reaction product—polybuthylmethacrylate (PBMA) are soluble in 2-propanol, monomer conversion level did not exceed 5–6% and semiconductor nanoparticles sizes were within 2.5–25 nm, one

* Corresponding author. Tel.: +38-44-265-6295; fax: +38-44-265-6295.
E-mail addresses: alstr@ukr.net (A.L. Stroyuk), photochem@ukrpost.net (V.M. Granchak), photochem@ukrpost.net (A.V. Korzhak), stephan@ukr.net (S.Ya. Kuchmii).

1010-6030/$ – see front matter © 2004 Elsevier B.V. All rights reserved.
doi:10.1016/S1010-6030(03)00371-X

can assume that BMA photopolymerization proceeded virtually in homogeneous solutions in contrast to analogous heterogeneous systems described in [8–10].

2. Experimental

2.1. Materials

2-Propanol (pure grade) was boiled over calcinated CaO for water removal, then distilled twice. BMA was washed with 20% solution of NaOH and distilled water, then dried with anhydrous $CaCl_2$ and distilled at reduced pressure at 60–80 °C. Pure monomer was stored in dark at 7–10 °C. Ferric nitrate (analytically pure) was purified through recrystallization. Other chemicals ($Zn(CH_3COO)_2$ (analytically pure), NaOH (pure), $Cd(CH_3COO)_2$ (analytically pure), $Na_2S{\cdot}9H_2O$ (analytically pure, Aldrich)), as well as dyes—sodium salts of fluorescein (analytically pure), tetrachlorofluorescein (THF, analytically pure), tetrabromofluorescein (TBF, analytically pure), tetraiodofluorescein (TIF, analytically pure) and tetrachlorofluorescein (THTIF, analytically pure)—were used without extra purification.

2.2. Instruments

Absorption spectra of solutions in UV and visible spectral domains (250–710 HM) were recorded on "Specord UV-Vis" spectrophotometer. Time-resolved photolysis experiments were carried out in micro-millisecond time range. Schematic diagram of the kinetic flash spectrophotometry setup can be found in [15]. Irradiation of solutions was carried out with two xenone flash lamps by the light with $\lambda > 460$ nm. Duration of pulse did not exceed 40 μs and their intensity was varied from 5×10^{15} to 25×10^{15} quanta per pulse. The non-stationary differential absorbance (ΔD_0) was measured after complete decay of excitatory pulse. Probing was carried out with the focused beam of light from a 175 W incandescend lamp. The values of non-stationary absorbance were determined in 400–700 nm range with the use of a photomultiplier, the signals form which were passed through analog-digital converter integrated with PC. Measurements were carried out in glass 7 cm cuvettes with internal diameter of 1.1 cm. The life-times ($\tau = 1/k_I$) and rate constants of triplet-excited dyes deactivation (k_I), which was found to be first-order process, were calculated from the slope of the linear relations $\ln(\Delta D_t) - f(t)$. For the estimation of the life-times of other intermediates of dyes photolysis with more complex decay kinetics their half-lives ($t_{1/2}$) values were used.

2.3. Photopolymerization rate measurements

BMA photopolymerization was studied with the use of dilatometry by measuring the fall of meniscus height change in the dilatometer which is directly proportional to the reaction rate. The values of the photopolymerization rates were calculated from the following formula:

$$R_p = 100\pi \frac{r^2 \Delta h[M]}{FVf\tau}$$

where r is the radius of the capillary of the dilatometer (cm); Δh-a change in the height of the meniscus (cm) in the course of photopolymerization after the irradiation during τ seconds; $[M]$-the molar monomer concentration; F-the volume contraction of the monomer (for BMA, $F = 19.7\%$); V-the volume of a solution in the dilatometer (ml); f-the volume fraction of the monomer in a solution.

Dilatometers were composed of cylindric glass cuvettes 3 cm in diameter to which capillaries 0.3–0.5 mm in diameter were attached. Solutions were irradiated with the light of the mercury high-pressure 1000 W lamp "DRSh-1000" with $\lambda = 310$–370 nm or with the light from 500 W incandescent lamp with $\lambda > 460$ nm using appropriate filters combinations. The light intensity was adjusted with the use of calibrated metallic meshes. Ferrioxalate actinometry was used for the measuring of the light intensity of the mercury lamp. Before dilatometric measurements and flash photolysis, cuvettes with solutions were degassed on a high-vacuum apparatus using at least five freeze–vacuum–thaw cycles.

2.4. Determination of the molecular weight of the polymer

The average molecular weight (M_w) of PBMA was determined by viscosimetry. PBMA was precipitated by ethanol, washed with the same solvent, dried and after the weighing dissolved in benzene. The intrinsic viscosity of the resulting polymer solution was determined using Ostwald viscometer with the accuracy within 15%.

2.5. CdS colloids synthesis

The nanosized cadmium sulfide was synthesized by the reaction between cadmium acetate and sodium sulfide in 2-propanol. For this purpose, 1 ml of $Cd(CH_3COO)_2$ solution (0.05 M) was diluted with the same solvent to 47 ml and 2.5 ml of a Na_2S solution in 2-propanol (0.01 M) was added dropwise under vigorous stirring. As a result, we obtained colloidal solutions with molar CdS concentration 5×10^{-4} M. Cadmium acetate excess (5×10^{-4} M) presented in solutions played role of the stabilizer of CdS colloidal particles. To obtain cadmium sulfide particles of different sizes, we varied the temperature at which the synthesis was conducted. The specific rates (per square meter of the surface of colloidal particles) of the BMA photopolymerization induced by CdS nanoparticles were determined by dividing the values characterizing the overall reaction rates by the total surface area of the CdS particles in solution. The latter

values were estimated from cadmium sulfide concentration and the average particle diameter assuming that during the synthesis, ultrasmall spherical CdS crystals are formed with a density of 4.82 g cm^{-3}.

2.6. ZnO nanoparticles synthesis

ZnO colloids were synthesized according to [16,17] through slow mixing of the solutions of $Zn(CH_3COO)_2$ and KOH in 2-propanol at 0 °C. Resulting colloidal solutions were aging for 2 h at 60–65 °C and kept in dark at 5–10 °C. Similar procedure was used to prepare colloidal solutions of other metal oxides in 2-propanol, such as CdO, PbO, CuO, Cu_2O, Ag_2O.

2.7. Ferric oxide colloids synthesis

Colloidal iron(III) oxide solutions were obtained by forced hydrolysis upon dissolving ferric nitrate nonahydrate in 2-propanol. Resulting iron oxide sols retain stability during several months if maintained at 5–10 °C and coagulate rapidly at the temperatures exceeding 20 °C. It was noted that colloidal Fe_2O_3 solution retains its stability at room temperature for a long period in the presence of BMA monomer. Ferric oxide was prepared also in water according to the well-known techniques [18–20] to identify the colloid formed in the alcohol. Heating a solution of ferric nitrate at reflux for 1.0–1.5 h leads to a yellow-brown colloidal solution with the composition corresponding to the formula $Fe_2O_3 \cdot xH_2O$ [21]. X-rays diffraction experiments on the coagulants of the colloids synthesized both in water and in 2-propanol showed a lack of crystal structure.

Table 1
Spectral and energy characteristics of CdS, ZnO and Fe_2O_3 nanoparticles

Semiconductor	d (nm)	E_g (eV)	E_{CB} (V)	E_{VB} (V)
ZnO	5.0	3.55	−0.30	+3.25
CdS	6.0	2.60	−1.00	+1.60
CdS	3.0	2.80	−1.15	+1.65
CdS	2.5	3.00	−1.30	+1.70
Fe_2O_3	3.25	2.05	−0.50	+1.55

Notes: potentials values are given for pH 7 relatively to NHE; d-the average diameter of semiconductor particles.

3. Results and discussion

3.1. Absorption spectra and characterization of semiconductor nanoparticles

3.1.1. Cadmium sulfide colloids

Absorption spectra of CdS colloidal solutions in 2-propanol are given in Fig. 1a. As can be seen, at a decrease in the synthesis temperature the edge of long-wave absorption band of CdS colloid undergoes a hypsochromic shift, thus indicating on quantum confinement effects evolution in synthesized CdS nanoparticles [11,12]. The average diameters of CdS nanoparticles synthesized at 25, 0 and −88 °C as well as its energy characteristics are given in Table 1. Band gap values (E_g) of semiconductor nanoparticles were estimated from the edge of the long-wave absorption bands in electronic spectra of CdS colloids [11,22], the average particles sizes were estimated with the use of well-known correlation [22] between E_g and the average diameter of CdS particles. The potentials of the top of the valence band (E_{VB}) and the bottom of the conduction band (E_{CB}) were estimated within the effective masses approximation using

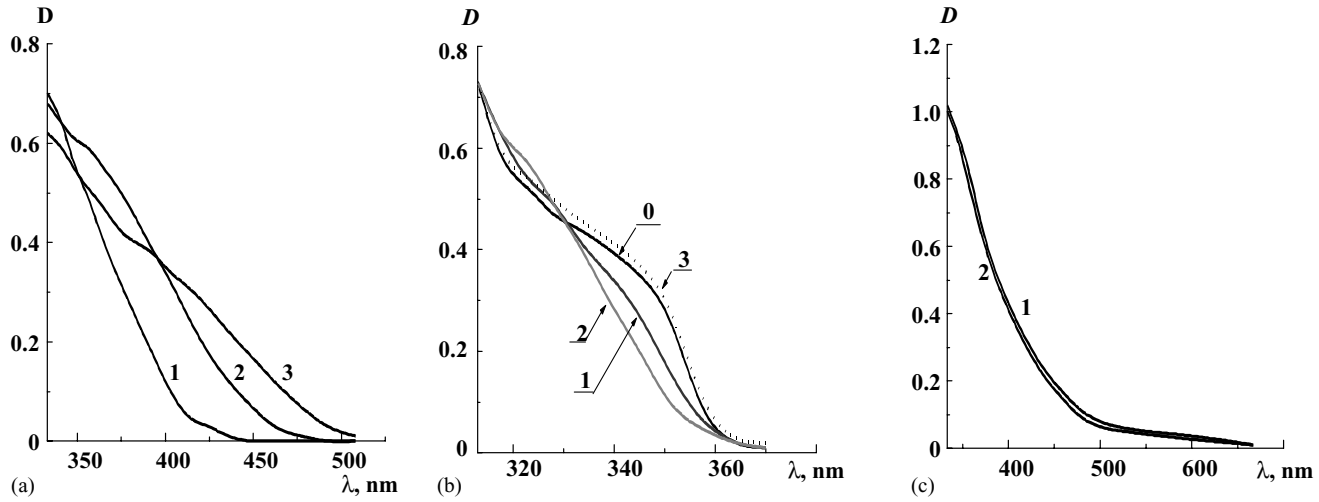

Fig. 1. Absorption spectra of CdS, ZnO and Fe_2O_3 colloidal solutions in 2-propanol. (a) Absorption spectra of CdS colloids in 2-propanol. Temperature of the synthesis: (1) −88 °C; (2) 0 °C; (3) +25 °C. [CdS] = 5×10^{-4} M, optical path d = 1 cm. (b) Hypsochromic shift of the absorption band edge in the spectrum of deaerated ZnO colloid in 2-propanol under stationary irradiation with λ = 310–370 nm. [ZnO] = 1×10^{-3} M, colloidal solution spectrum before irradiation (0), after 15 min of irradiation (1), after 30 min of irradiation (2), spectrum of the solution (2) after air admission (3). Light intensity $I = 3.6 \times 10^{18}$ quanta s^{-1}, d = 1 cm. (c) Absorption spectra of $Fe_2O_3 \cdot xH_2O$ colloids in 2-propanol (1) and water (2). [Fe_2O_3] = 5×10^{-4} M, d = 1 cm.

the values of CdS electrons effective mass $m_e^* = 0.2$ and holes effective mass $m_h^* = 0.8$ [22,23] and taking into account the flat-band potential for massive monocrystal CdS $U_{FB} = -0.66$B (relative to the normal hydrogen electrode, NHE).

3.1.2. Zinc oxide colloids

An absorption band with steep long-wave edge at 350–355 nm (corresponding to $E_g = 3.55$ eV) is characteristic feature of the electronic absorption spectra of ZnO colloids in 2-propanol (see Fig. 1b). According to [16,17], such absorption bands are inherent in ZnO colloids with the average particles diameters within 5.0 ± 0.5 nm range. Energy characteristics of ZnO nanoparticles—E_{CB} and E_{VB} (see Table 1)—were estimated with the use of the correlations between these values and the average size of ZnO particles [24].

It was found that the irradiation of a degassed ZnO colloidal solution in 2-propanol with 310–390 nm light causes a hypsochromic shift of the edge of its absorption band (see Fig. 1b). Such behaviour of the colloid is connected with dynamic Burstein effect [16,25], i.e. accumulation of excess electrons on ZnO nanoparticles, which is possible due to fast capture of the photogenerated ZnO valence band holes by alcohol molecules:

$$ZnO + h\nu \rightarrow ZnO(e_{CB}^- + h_{VB}^+) \quad (1)$$

$$h_{VB}^+ + (CH_3)_2CHOH \rightarrow (CH_3)_2C^{\bullet}OH + H^+ \quad (2)$$

where e_{CB}^- is the conduction band electron, h_{VB}^+ is the valence band hole.

Excess electrons accumulation on the lowest levels near the bottom of the ZnO conduction band leads to an increase in the energy necessary for the photogeneration of the ensuing electron–hole pairs and thus causes the spectral changes observed in ZnO colloids absorption spectra. No hypsochromic shifts of the ZnO absorption band position is observed in the presence of air oxygen or BMA due to rapid withdrawal of the electrons accumulated in the conduction band of ZnO nanoparticles as follows:

$$e_{CB}^- + O_2 \rightarrow O_2^{\bullet -} \quad (3)$$

$$e_{CB}^- + H^+ \rightarrow H^{\bullet} \quad (4)$$

$$M + H^{\bullet} \rightarrow HM^{\bullet} \quad (5)$$

where M denotes the monomer molecule.

It should be noted that direct interaction between the electrons, photogenerated in ZnO nanoparticles, and BMA molecules is quite improbable because BMA reduction potential $E_{BMA}^{red} \approx -1.1$B, whereas ZnO conduction band potential at pH 7 $E_{CB} = -0.20$ B (NHE). The possibility of the reduction of H^+ by ZnO conduction band electrons (*reaction* 4) was proved by the evolution of molecular hydrogen at prolonged irradiation of degassed ZnO colloids in 2-propanol in the presence of high-dispersed palladium.

3.1.3. Iron(III) oxide colloids

Absorption spectra of colloidal solution of ferric oxide in 2-propanol are given in Fig. 1c. As can be seen, spectra of colloidal Fe_2O_3 forming by the hydrolysis of iron(III) nitrate both in water at 80–90 °C and in 2-propanol at 10–15 °C are almost coincident. According to [20], colloidal Fe_2O_3 particles forming in aqueous media at the above-described conditions have spherical shape, weakly pronounced crystal structure and substantial polydispersity, the bulk of the particles having sizes within 3–25 nm. Hence, a polydyspersed colloids of amorphous hydrated ferric oxide $Fe_2O_3{\cdot}xH_2O$ with the particles sizes within 3–25 nm are formed upon dissolving ferric nitrate in 2-propanol due to rapid hydrolysis. The band gap value of $Fe_2O_3{\cdot}xH_2O$ colloidal particles formed in 2-propanol estimated from the position of the long-wave edge of the absorption band of colloidal solution amounts to 2.05–2.10 eV, which is in accord with the value $E_g = 2.02$эВ for colloidal haematite (α-Fe_2O_3) determined in [19] by photoacoustic spectroscopy. According to [18], flat-band potential of α-Fe_2O_3 colloidal particles does not substantially depend on the pH of the medium and at pH 7 $U_{FB} \approx -0.3$ V (NHE). Taking into account, that E_{CB} of *n*-semiconductors (including haematite) lies 0.15 V under the U_{FB}, we may adopt $E_{CB} \approx -0.45$ V (NHE) for ferric oxide nanoparticles and, since $E_g \approx 2.1$ eV, $E_{VB} \approx +1.6$ V (NHE).

3.2. Effect of the nature of semiconductor photoinitiator on the BMA polymerization rate

By control tests we established that only trace amounts of polymer form when a solution of BMA in 2-propanol is exposed to the light with $\lambda = 310$–370 nm in the absence of photoinitiators. In the presence of semiconductor nanoparticles, BMA photopolymerization proceeds with comparatively high rates. Table 2 contains the results of the investigation of the effect of CdS nanoparticles of different size, ZnO, Fe_2O_3 and, for comparison, thoroughly studied molecular photoinitiator—benzophenone [1,2], on the rate of BMA photopolymerization in 2-propanol. As can be seen, nanoparticles of all of the listed semiconductors have substantially higher activity in the BMA polymerization photoinitiation as compared with benzophenone. We tested also other colloidal metal oxides as photoinitiators of BMA polymerization, but with the exception of PbO and Cu_2O (see Table 2) having small photocatalytic activity, other metal oxides (CuO, CdO, Ag_2O) turned out to be inert in the photopolymerization initiation.

It should be stressed that colloidal particles of hydrous ferric oxide can initiate BMA polymerization at the irradiation with a portion of the visible light ($\lambda_{irr} = 400$–600 nm). The average molecular weight of PBMA formed in the presence of the investigated semiconductor nanoparticles is close to 1×10^6. As can be drawn from the data given in Table 2, the rate of BMA photopolymerization in the presence of CdS nanoparticles increases substantially at the decrease in the

Table 2
The effect of the nature of a photoinitiator (*P*), the average diameter of semiconductor particles (*d*), concentration of photoinitiator ([*P*]), the presence of sensitizers (*S*) and their concentration ([*S*]), irradiation wave length (λ_{irr}) and the light intensity (I_0) on the rate (R_p) and specific rate (R_p^s) of buthylmethacrylate (BMA) photopolymerization in 2-propanol

P	$[P] \times 10^4$ (M)	*d* (nm)	*S*	$[S] \times 10^5$ (M)	λ_{irr} (nm)	$I \times 10^{17}$ (quanta s^{-1})	$R_p \times 10^5$ (M c^{-1})	$R_p^s \times 10^4$ (M s^{-1} m^{-2})
–	–	–	–	–	365	36	0.02	–
BPh	10	–	–	–	365	36	0.40	–
CdS	2.5	6.0	–	–	365	36	1.81	2.4
CdS	2.5	3.0	–	–	365	36	2.42	2.3
CdS	2.5	2.5	–	–	365	36	5.51	4.5
CdS	2.5	6.0	–	–	λ > 400	24	1.23	1.4
CdS	2.5	3.0	–	–	λ > 400	24	1.40	1.3
CdS	2.5	2.5	–	–	λ > 400	24	2.61	2.0
ZnO	2.5	5.0	–	–	365	36	1.40	–
PbO	5.0	–	–	–	365	36	0.80	–
Cu_2O	1.0	–	–	–	365	36	0.20	–
Fe_2O_3	0.2	3–25	–	–	365	2.0	1.80	–
Fe_2O_3	0.2	3–25	–	–	440	0.8	0.52	–
Fe_2O_3	0.2	3–25	–	–	580	0.3	0.12	–
Fe_2O_3	0.8	3–25	–	–	365	2.0	2.00	–
Fe_2O_3	0.8*	3–25	–	–	365	2.0	0.60	–
–	–	–	F	2.0	λ > 460	–	0.19	–
–	–	–	TCF	2.0	λ > 460	–	0.32	–
–	–	–	TBF	2.0	λ > 460	–	0.45	–
–	–	–	TIF	2.0	λ > 460	–	0.58	–
–	–	–	TCTIF	2.0	λ > 460	–	0.62	–
ZnO	10.0	5.0	–	–	365	2.0	1.58	–
ZnO	10.0	5.0	F	2.0	λ > 460	–	1.52	–
ZnO	10.0	5.0	TCF	2.0	λ > 460	–	1.34	–
ZnO	10.0	5.0	TBF	2.0	λ > 460	–	1.13	–
ZnO	10.0	5.0	ТИФ	2.0	λ > 460	–	0.92	–
ZnO	10.0	5.0	TCTIF	2.0	λ > 460	–	0.88	–

Notes: BPh: benzophenone; in all cases [BMA] = 3.15 M.
*– in the presence of water, $[H_2O] = 0.02$ M.

average diameter of nanoparticles. The observed increase in the rate cannot be explained by a simple increase in the external surface area when the CdS particles diameter decreases, since as we see from the data in Table 2, as we go to CdS particles with diameter 2.5 nm, characterized by the maximum surface area, not only the overall rate of the process but also the specific rate (per square meter) increases. We suggest that the observed increase in the photopolymerization rate as the CdS particles diameter decreases is connected with the manifestation of quantum confinement effects, i.e. with the difference in the energy characteristics of CdS nanoparticles of different size (see Table 1). In fact, if we adopt the BMA reduction potential in 2-propanol to be close to methylmethacrylate reduction potential in the same solvent (−1.1 V, NHE [9]), we may conclude that BMA molecules can efficiently accept conduction band electrons only from the smallest of the CdS nanoparticles studied −2.5 nm in diameter. As a result of this reaction monomer anion-radicals ($M^{\bullet -}$) are formed, which further can transform in protic alcohol medium into electroneutral radicals ($HM^{\bullet}$), the latter initiating BMA polymerization chains:

$$e_{CB}^- + M \rightarrow M^{\bullet -} \quad (7)$$

$$M^{\bullet -} + H^+ \rightarrow HM^{\bullet} \quad (8)$$

The possibility of monomer radicals generation with the participation of CdS conduction band electrons may apparently serve as a reason for the advanced photocatalytic activity of cadmium sulfide nanoparticles with the average diameter of 2.5 nm. It should be noted that in the presence of CdS nanoparticles of larger diameter, as well as ZnO and Fe_2O_3 nanoparticles, can occur also indirect monomer activation via atomic hydrogen formation (*reactions* 4 *and* 5), but the efficiency of radicals generation in that way should be apparently smaller, since the stationary concentration of the protons formed in *reaction* 2 cannot be sufficiently high as compared with monomer concentration.

3.3. Kinetic regularities of BMA photopolymerization

Analysis of [1–10] indicates that the alkylmethacrylates polymerization induced by photoinitiators of different nature proceeds via free radical mechanism. Free radical polymerization rate can be expressed by Eq. (I), if we adopt the main chain termination process to be macroradicals recombination:

$$-\frac{d[M]}{dt} = R_p = \frac{k_p}{k_t^{0.5}}\sqrt{V_{in}}[M] \quad (I)$$

where R_p is the overall polymerization rate, V_{in}-the initiation rate, k_p-the rate constant of chain propagation, k_t-the rate constant of chain termination [M]-the molar monomer concentration.

In the presence of a photoinitiator the chain initiation rate can be determined from the following expression:

$$V_{in} = \beta[P]I \quad \text{(II)}$$

where β is the photoinitiation quantum yield, [P]-a photoinitiator concentration, I-the light intensity.

The overall photopolymerization rate may be expressed as follows:

$$R_p = \frac{k_p \beta^{0.5}}{k_t^{0.5}}[M]\sqrt{[P]V_{in}I} \quad \text{(III)}$$

Expression (III) shows that in the case of free radical photopolymerization the values of kinetic orders for photoinitiator and monomer concentrations as well as the light intensity are equal to 0.5, 1.0 and 0.5, correspondingly.

To establish kinetic dependences and a possible mechanism for BMA photopolymerization induced by semiconductor nanoparticles, we tried to establish how the photocatalysts and monomer concentrations and the light intensity effect the rate of this process.

It was found that the rate of BMA photopolymerization in the presence of CdS, ZnO and Fe_2O_3 nanoparticles increases at an increase in the intensity of excitatory light (I_0), monomer, ZnO and CdS nanoparticles concentrations. Calculated reaction orders of the light intensity (I) (n_3) and [M] (n_1), as well as of ZnO and CdS concentrations (n_2) were found to be close to the corresponding parameters of theoretical kinetic Eq. (III) for all of the studied semiconductor photoinitiators (see Table 3). This fact and also a number of other factors including quenching of the photopolymerization by molecular oxygen, the absence of "dark" post-reactions, allows the conclusion that the photopolymerization of BMA in 2-propanol induced by CdS, ZnO and Fe_2O_3 nanoparticles proceeds via *free radical mechanism*. The larger value of experimental reaction order of monomer concentration as compared with theoretical value can be connected with the chain termination with the participation of $HM^{\bullet}$ radicals [10]:

$$HM_n^{\bullet} + HM^{\bullet} \rightarrow H_2M_{n+1} \quad (9)$$

Some decrease in the value of the reaction order of the light intensity as compared with theoretical value (0.5) can be explained by non-linear increase in the efficiency of the recombination of photogenerated charge carriers with an increase in the irradiation intensity, as it was established, for example, for ZnO nanoparticles [27].

The dependence of BMA photopolymerization rate on the concentration of Fe_2O_3 is a curve displaying a maximum (see Fig. 2a). We should note the minor growth of the reaction rate with increasing the concentration of the photoinitiator as compared with the value expected from the theoretical kinetic Eq. (III). Fig. 2a shows that the four-fold increase in iron(III) oxide concentration (from 2×10^{-5} to 8×10^{-5} M) leads to an increase in rate of merely ~10% instead of the expected two-fold increase. Furthermore, further increase in the Fe_2O_3 concentration leads to a decrease in the BMA photopolymerization rate. This effect cannot be attributed to internal light filtration by iron(III) oxide nanoparticles, since light absorption by the solutions was not complete even at the maximum colloid concentration used. The observed

Table 3
Kinetic orders of buthylmethacrylate photopolymerization in 2-propanol in the presence of colloidal CdS, ZnO, Fe_2O_3 nanoparticles

Photoinitiator (P)	d (nm)	$R_p = k[P]^{n1} I^{n2}[BMA]^{n3}$		
		n_1	n_2	n_3
ZnO	5.0	0.55	0.40	1.25
CdS	2.5	0.50	0.35	1.55
CdS	3.0	–	–	–
CdS	6.0	–	–	–
Fe_2O_3	3–25	–	0.50	1.40
ZnO + TCF	–	0.50	0.40	1.00

Notes: d: the average diameter of semiconductor nanoparticles; TCF: tetrachlorofluorescein. Values determination accuracy ±0.02.

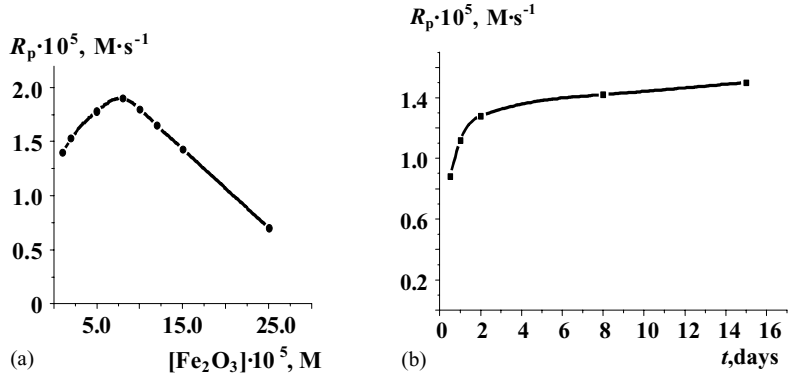

Fig. 2. Dependence of the rate of buthylmethacrylate photopolymerization in 2-propanol on $Fe_2O_3 \cdot xH_2O$ concentration (a) and aging time of the colloid (b). $[Fe_2O_3] = 1.0 \times 10^{-4}$ M, [BMA] = 3.15 M, λ_{irr} = 310–370 nm, $I = 2.0 \times 10^{17}$ quanta s^{-1}.

kinetics may be related to a decrease in the initiation efficiency with increasing concentration of the photoinitiator due to an increase in the role of side reaction involving annihilation of primary 1-hydroxymethylethyl radicals entering the bulk of the solution on the Fe_2O_3 particles:

$$(CH_3)_2C^{\bullet}OH + (Fe_2O_3)n \cdot xH_2O \rightarrow H^+ + (CH_3)_2CO + (Fe^{II}Fe^{III}O_3)(Fe_2O_3)_{n-1} \cdot xH_2O \quad (10)$$

The possibility of such redox-process with the participation of 1-hydroxymethylethyl radicals and Fe_2O_3 colloidal particles was demonstrated in a γ-radiolysis experiments [8]. We should note that after irradiation of the solutions, we observed slight increase in the optical density over the entire visible spectrum, which may be attributed to the appearance of traces of iron(II) hydroxide in the bulk of semiconductor [13].

The data given in Table 2 indicate that water significantly inhibits the photoactivity of Fe_2O_3 nanoparticles. We assumed that the water molecules having better adsorption affinity to the surface of iron(III) oxide than 2-propanol molecules inhibit oxidation-reduction reactions of the photogenerated valence band holes with the alcohol. Large increase in photoactivity of the Fe_2O_3 nanoparticles observed upon the storage ("aging") of the colloid was attributed to the reverse process involving the gradual removal of water molecules by 2-propanol present in a solution in large excess (see Fig. 2b).

3.4. Sensitization of ZnO nanoparticles to the visible light

Among the studied nanosized semiconductor photoinitiators of BMA polymerization, colloidal ZnO particles stand out for their high photocatalytic activity in the reaction under investigation, thoroughly studied photophysical characteristics and relative simplicity of preparative procedure. The principle disadvantage of the photopolymerization compositions based on ZnO nanoparticles is their insensitivity to the visible light (λ_{irr} = 400–800 nm). One of the ways of the expansion of the light sensitivity spectral region of wide-band gap semiconductors, specifically ZnO, is their sensitization with dyes of different nature [28,29]. Our attempts to sensitize ZnO nanoparticles in BMA photopolymerization to the visible light with dyes of various structure (xanthene, anthraquinone, tritane, thiazine dyes and their derivatives) revealed that the most effective sensitizers of nanosized ZnO are fluorescein and a number of its halogenated derivatives (see Fig. 3a and Table 2). As can be derived from the data given in Table 2, in the presence of the above-mentioned dyes under the irradiation with the light of incandescent lamp ($\lambda > 460$ nm), BMA photopolymerization rates approach to the values obtained at the interband excitation of ZnO nanoparticles with the near-UV light with λ = 310–370 nm.

In the presence of fluorescein and its halogenated derivatives in the systems, which do not contain ZnO nanoparticles, BMA photopolymerization proceeds with small rates under the irradiation with the visible light ($\lambda > 460$ nm), the

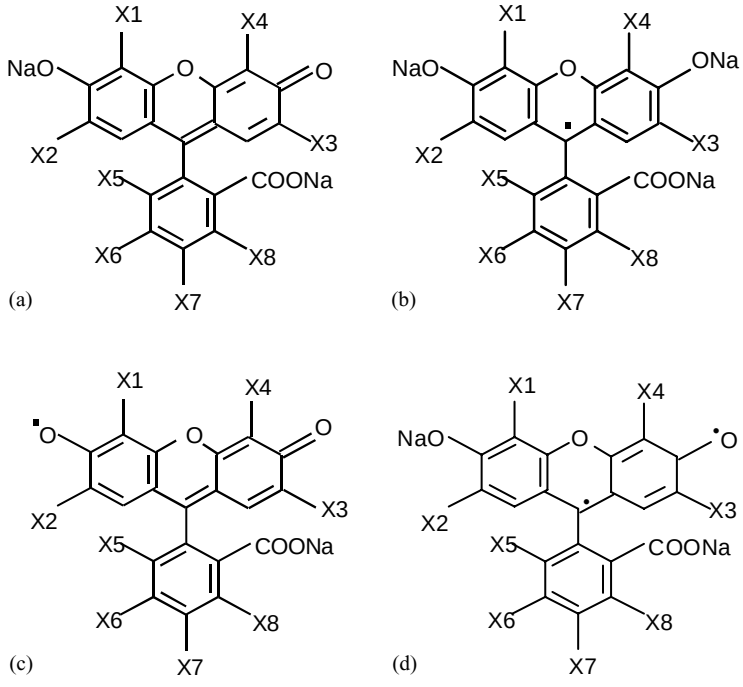

Fig. 3. Structures of fluorescein and some of its halogenated derivatives in ground state (a), in one-electron-reduced form (b), in one-electron-oxidized form (c), in triplet-excited state (d) [32,33]. Substituents designation for different dyes: fluorescein ($X_{1–8}$ = H), tetrachlorofluorescein ($X_{1–4}$ = Br, $X_{5–8}$ = H), tetrabromofluorescein ($X_{1–4}$ = Br, $X_{5–8}$ = H), tetraiodofluorescein ($X_{1–4}$ = I, $X_{5–8}$ = H), tetrachlorotetraiodofluorescein ($X_{1–4}$ = *I*, $X_{5–8}$ = Cl).

polymerization rate increases in the consequence TCTIF > TIF > TBF > TCF > F (see Table 2), which correlates with the efficiency of the intercombinatory conversion of the singlet-excited states of these dyes into the triplet states [15]. Such dependence shows that the initiation stage of the photopolymerization involves the triplet states of the dyes or the radicals formed from them.

Injection of the ZnO nanoparticles into a reacting mixture containing a dye leads to considerable increase in the rate of BMA photopolymerization induced by the light with $\lambda >$ 460 nm, but in this case we observed another dyes activity consequence, namely F > TCF > TBF > TIF > TCTIF (see Table 2). As in the case of the BMA polymerization induced only by ZnO nanoparticles so in the presence of ZnO and sensitizers we observed linear increase in the photopolymerization rate at an increase in ZnO and monomer concentrations and light intensity. Parameters of kinetic equation of the photopolymerization, i.e. reaction orders of [ZnO], [*M*] and *I* are given in Table 3. The dependence of BMA photopolymerization rate on dye concentration given in Fig. 4a has more complicated form. The photopolymerization rate growth at an increase in sensitizer (by the example of TCF) concentration to 3.5×10^{-5} M may be explained by an increase in the fraction of absorbed light, while the decrease in the rate of photopolymerization on further increase of the content of the sensitizer in a solution is evidently caused by self-quenching of the excited state of the dye as a result of the interaction of dye molecules in excited states with dye molecules in ground state. The same character of the dependence of the photopolymerization rate on the dye concentration both in the absence of ZnO and in the presence of the latter speaks in favour of such explanation. Another factor which may cause a decrease in the photopolymerization rate at an increase in a sensitizer concentration may lie in formation of associated forms of the dyes but the invariability of the position of absorption anf fluorescence bands of halogenated derivatives of fluorescein in 2-propanol at an increase of their concentration indicates on small extent of dyes association in studied systems.

3.5. The effect of a sensitizer nature on the BMA photopolymerization rate in the presence of ZnO nanoparticles

In accordance with the theory of electron transfer from a dye molecule adsorbed on the surface of semiconductor particles or localized within the nanoparticles adsorption layer, the dependence of the electron transfer rate constant (k_{ET}) on energy gap (ΔE) between the energy levels of excited dye and the bottom of the conduction band of a semiconductor may be defined as follows [30]:

$$k_{ET} = C\sqrt{\Delta E - \lambda} \quad \text{(IV)}$$

where λ is the reorganization energy of electron system of semiconductor upon electron transfer, *C* is a constant, $C = \sigma_0(2m_e)^{3/2}\nu^2/\pi\hbar^4$, where σ_0 is the volume of lattice unit of semiconductor crystal, m_e is an electron rest mass, *h* is reduced Planck constant, ν the exchange energy of electron transfer.

Thus, for one and the same semiconductor, when $\lambda =$ const, the theory predicts linear dependence between the rate of electron transfer from a dye to a semiconductor and the square root of the gap between the potential of a dye in excited (singlet or triplet) state and the potential of the bottom of the conduction band of a semiconductor. Fig. 4b depicts the dependence between the BMA photopolymerization rate in the presence of studied dyes and $(E_T)^{1/2}$, where E_T is the energy of the first triplet level of dyes (taking into account

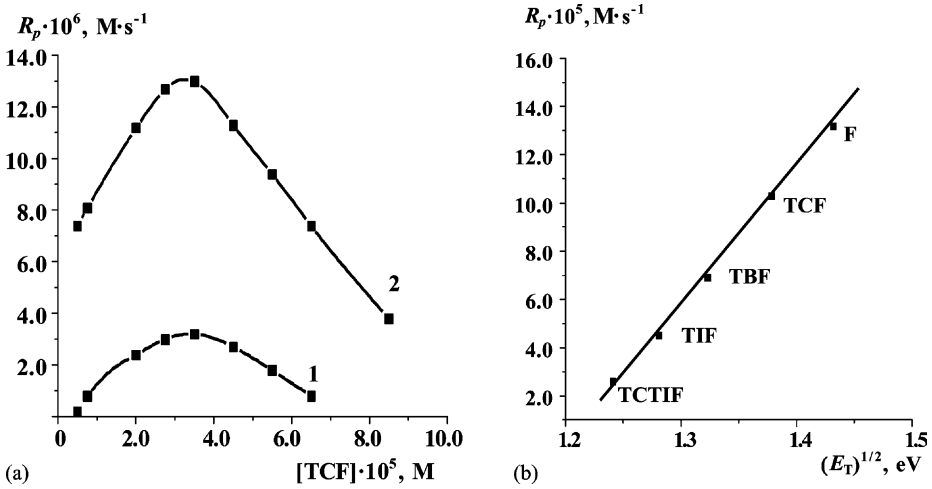

Fig. 4. (a) Dependence of the rate of buthylmethacrylate (BMA) photopolymerization on tetrachlorofluorescein concentration. [BMA] = 3.15 M, $\lambda_{irr} >$ 460 nm: 1: in the absence of ZnO nanoparticles, 2: in the presence of ZnO nanoparticles. [ZnO] = 1×10^{-3} M. (b) Dependence of the rate of buthylmethacrylate photopolymerization in solutions containing ZnO nanoparticles and halogenated derivatives of fluorescein on the square root of the gap between the potential of the sensitizers in first triplet-excited state and the potential of the bottom of the conduction band of ZnO nanoparticles. [Dye] = 3.5×10^{-5} M, [ZnO] = 1×10^{-3} M, [BMA] = 3.15 M, $\lambda_{irr} >$ 460 nm.

that one and the same semiconductor was used in sensitization experiments—zinc oxide—we adopt $\lambda = \text{const} \approx 0$ as in [30]). The linear nature of the dependence found is in accord with above-stated theoretical considerations and indicates the determinant role of the rate of electron transfer from photoexcited dye to ZnO nanoparticles in photochemical initiation of BMA polymerization in the systems under investigation.

3.6. The study of a mechanism of ZnO nanoparticles sensitization

It is known that excessive energy of the lowest singlet-excited state of a dye molecule is lost via fluorescence, nonradiative degradation to the ground state and intercombination conversion (ICC) into the triplet state [15]:

$$S_1 \rightarrow T_1 \quad \text{(ICC)} \tag{11}$$

$$T_1 \rightarrow S_0 \quad \text{(monomolecular triplet deactivation)} \tag{12}$$

$$T_1 + S_0 \rightarrow S_0 + S_0$$
(self-quenching of triplet-excited dye) (13)

$$T_1 + T_1 \rightarrow S_1 + S_0 \quad \text{(triplet–triplet annihilation)} \tag{14}$$

Triplet self-quenching (*process* 13) becomes noticeable at sufficiently high dye concentrations. Simultaneously with the reactions 12–14, disproportionation of triplets can take place. This process is typical for dyes of different classes [15] and leads to the formation of one-electron-reduced (ORF, $D^{\bullet -}$, see Fig. 3b) and one-electron-oxidized (OOF, $D^{\bullet +}$, Fig. 3c) forms of a dye:

$$T_1 + T_1 \rightarrow D^{\bullet +} + D^{\bullet -} \tag{15}$$

Pulse photoexcitation of fluorescein and its halogenated derivatives results in short-lived reversible changes in their absorption spectra caused by the formation of short-lived intermediates—triplets, ORF and OOF of the dyes. In Fig. 5 as an example non-stationary absorption spectra of TCTIF are shown in which four signals can be distinguished: a broad absorption band at $\lambda > 560$ nm, narrow bands with maxima at 415 and 445 nm and a negative signal in the 470–550 nm region. Analogous spectra were observed at pulse photoexcitation of other sensitizers—F, TCF, TBF and TIF.

Analysis of the data given in [31–35] allows the assignment of the bands observed in non-stationary absorption spectrum given in Fig. 5. The broad structureless band at $\lambda > 560$ nm with a maximum at 600 nm arises from the light absorption by triplet TCTIF molecules resulting in the formation of higher triplet-excited states of the dye (T–T band). The peaks at $\lambda_{max} = 445$ and 415 nm belong to OOF and ORF of the TCTIF, correspondingly. The negative signal in the 470–550 nm region is caused by partial conversion of the dye into short-lived products (non-stationary bleaching of a dye).

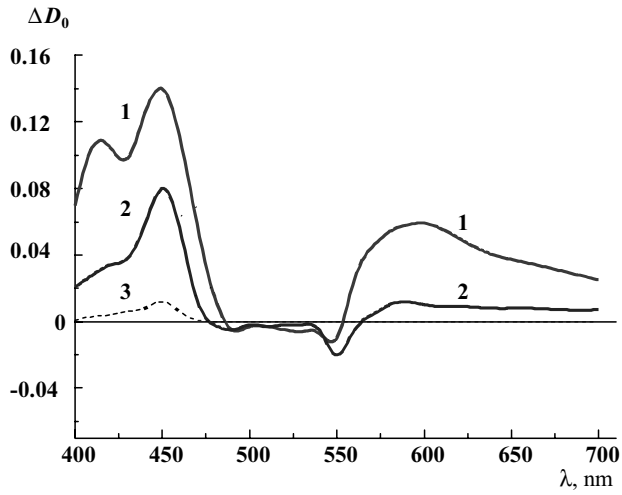

Fig. 5. Non-stationary differential absorption spectra of tetrachlorotetraiodofluorescein (TCTIF). (1) [TCTIF] = 2×10^{-5} M; (2) [TCTIF] = 2×10^{-5} M, [ZnO] = 1×10^{-3} M; (3) [TCTIF] = 2×10^{-5} M, [ZnO] = 1×10^{-3} M, air-saturated solution. $\lambda_{irr} > 460$ nm.

3.6.1. Triplet state of the sensitizers

In the presence of ZnO nanoparticles we observed substantial decrease both in the initial concentration of triplet-excited forms of the dyes (see Fig. 5) and in their life-time (see Table 4). We suggest that a decrease in triplet concentration in the presence of ZnO nanoparticles is caused by the appearance in this case of a new, concurrent to intercombinatory conversion (*process* 12) channel of singlet-excited dyes deactivation—electron transfer from the singlet to ZnO conduction band:

$$S_1 + \text{ZnO} \rightarrow D^{\bullet +} + \text{ZnO}(e^-_{CB}) \tag{16}$$

Participation of the singlet-excited dyes in the electron transfer to ZnO is confirmed by formation of the OOF of the dyes in air-saturated solutions when the signals of the triplets are not observed (see Fig. 5). Electron transfer from the singlet-excited dyes to the conduction band of ZnO nanoparticles is thermodynamically favourable since, for example, oxidation potential of the singlet-excited TCTIF is −1.3 V (NHE) [34], whereas ZnO conduction band potential equals to −0.2 V (NHE, pH 7). The reduction in the life-time of the triplets in the presence of ZnO nanoparticles (see Table 4) shows that some fraction of triplet dye molecules also participate in the electron transfer to ZnO:

$$T_1 + \text{ZnO} \rightarrow D^{\bullet +} + \text{ZnO}(e^-_{CB}) \tag{17}$$

3.6.2. One-electron-reduced forms of the dyes

The major portion of triplet-excited dye molecules are converted to ORF and OOF during the excitatory light pulse. ORF and OOF formation occurs apparently via reaction (15) at the interaction of two photoexcited dye molecules. This is confirmed by the fact that the initial concentrations of these intermediates depend on the square of the light intensity (see Fig. 6a). At the moment corresponding to the beginning of

Table 4
Characterization of photolysis intermediates of fluorescein and some of its halogenated derivatives

System	Triplet-excited state of a dye			ORF of a dye			OOF of a dye	
	T–T band position	τ_T (μs)	$k_I \times 10^{-4}$ (s^{-1})	λ_{max} (nm)	$t_{1/2}$ (μs)	E ($D/D^{\bullet -}$), V (NHE)	λ_{max} (nm)	$t_{1/2}$ (μs)
F	$\lambda > 520$ nm, $\lambda_{max} = 560$ nm	240	0.42	–	–	−1.12 [33]	430	>600
F + ZnO	$\lambda > 540$ nm, $\lambda_{max} = 600$ nm	80	1.25	–	–	–	430	>600
TCF	$\lambda > 550$ nm, $\lambda_{max} = 580$ nm	130	0.77	–	–	–	420	>600
TCF + ZnO	$\lambda > 550$ nm, $\lambda_{max} = 580$ nm	65	1.54	–	–	–	420	400
TBF	$\lambda > 530$ nm, $\lambda_{max} = 570$ nm	130	0.77	410	450	–	440	350
TBF + ZnO	$\lambda > 530$ nm, $\lambda_{max} = 570$ nm	110	0.91	410	210	–	440	200
TIF	$\lambda > 550$ nm, $\lambda_{max} = 590$ nm	95	1.05	415	230	–	440	170
TIF + ZnO	$\lambda > 550$ nm, $\lambda_{max} = 590$ nm	60	1.67	415	100	–	440	130
TCTIF	$\lambda > 560$ nm, $\lambda_{max} = 600$ nm	90	1.11	415	250	−0.51 [33]	445	250
TCTIF + ZnO	$\lambda > 560$ nm, $\lambda_{max} = 600$ nm	55	1.82	415–420	140		445	170

Notes: F: fluorescein; TCF: tetrachlorofluorescein; TBF: tetrabromofluorescein; TIF: tetraiodofluorescein; TCTIF: tetrachlorotetraiodofluorescein; ORF, OOF: one-electron-reduced and one-electron-ozidized forms of a dye correspondingly. Literature data are given in italic type, τ_T determination accuracy is ±5 μs, $t_{1/2}$: ±10 μs. *Experimental conditions*: [S] = 2×10^{-5} M, [ZnO] = 1×10^{-3} M, pulse intensity: 15×10^{15} quanta per pulse.

the non-stationary signal registration ($t = 40$ μs) insignificant amount of the triplets remains in the system so that only physical triplets deactivation is observed (our estimations showed that the rate of this monomolecular process is an order of magnitude greater than that of the second order process of OOF and ORF formation requiring the collision of two excited dye molecules in solution in which the concentration of the triplets is very small).

The decay of the ORF cannot be described by either first-order or second-order equations—it corresponds to more complex kinetic relationship. According to [33,35], ORF of the dyes are consumed in reactions of dimerization and recombination with OOF:

$$D^{\bullet +} + D^{\bullet -} \rightarrow S_0 + S_0 \quad (18)$$

In the presence of ZnO nanoparticles, the initial concentration of ORF is decreased by an order of magnitude while its decay rate is doubled (see Table 4), and is also described by complex kinetic dependence. We associate the decrease in the initial ORF concentration in the presence of ZnO nanoparticles with the electron transfer from singlet- and triplet-excited dye molecules to the semiconductor nanoparticles (*reactions* 16 *and* 17), concurrent to the reaction (15). Shortening of the ORF life-times in the presence of ZnO nanoparticles may be explained by the electron transfer from ORF into ZnO conduction band which is thermodynamically favourable (see data given in Table 4):

$$D^{\bullet +} + ZnO \rightarrow S_0 + ZnO(e^-_{CB}) \quad (19)$$

3.6.3. One-electron oxidized forms of the dyes

As noted before, in the absence of ZnO nanoparticles OOF of the dyes form during the excitatory flash via the interaction of the two photoexcited dye molecules (*reaction* 15). This is confirmed by the dependence of the initial OOF

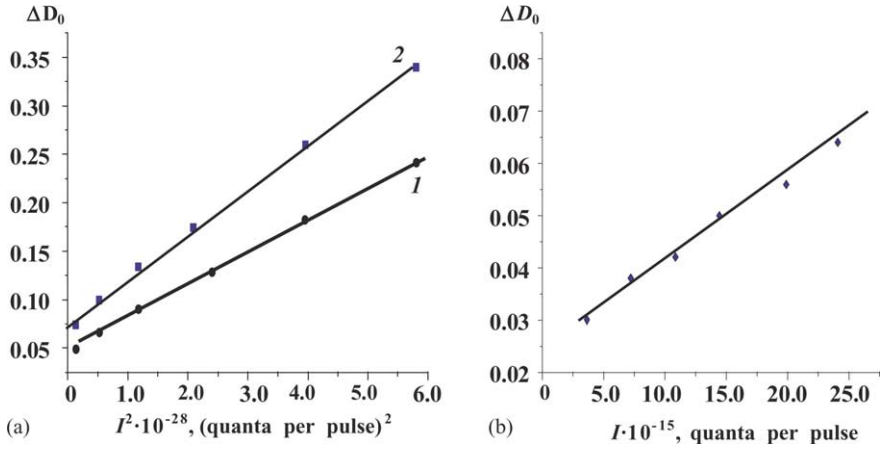

Fig. 6. (a) Dependence of the initial concentration of one-electron-reduced form (1) and one-electron-oxidized form (2) of tetrachlorotetraiodofluorescein (TCTIF) on the square of the intensity of excitatory pulse in the absence of ZnO nanoparticles. $d = 7$ cm, [TCTIF] = 5×10^{-6} M. (b) Dependence of the initial concentration of one-electron-oxidized form of tetracholrotetraiodofluorescein (TCTIF) on the intensity of excitatory pulse in the presence of ZnO nanoparticles. $d = 7$ cm, [TCTIF] = 5×10^{-6} M, [ZnO] = 1×10^{-3} M.

Table 5
Monomer effect on the life-times of triplets (T_T), one-electron-reduced (ORF) ($\tau_{D^{\bullet-}}$) and one-electron-oxidized (OOF) ($\tau_{D^{\bullet+}}$) forms of tetrachlorotetraiodofluorescrein (TCTIF) in the absence and in the presence of ZnO nanoparticles

[BMA] (M)	[ZnO] = 0			[ZnO] = 1 × 10^{-3} M		
	T_T	$\tau_{D^{\bullet-}}$	$\tau_{D^{\bullet+}}$	T_T	$\tau_{D^{\bullet-}}$	$T_{D^{\bullet+}}$
0	90	250	250	55	140	170
0.05	85	310	220	60	150	250
3.15	90	300	210	55	150	240

Notes: [TCTIF] = 2 × 10^{-5} M.

(as well as ORF) concentration on the square of the light intensity (see Fig. 6a). In the presence of ZnO nanoparticles, on the contrary, we observed linear increase in the initial concentration of OOF at an increase in the light intensity (see Fig. 6b). This indicates the participation of only one excited dye molecule in the formation of OOF. We suggest that in this case OOF of the dyes is formed as a result of the electron transfer from singlet- and triplet-excited molecules of the sensitizers into the conduction band of ZnO nanoparticles (*processes* 16 *and* 17). OOF decay may be described in all cases by complex dependence and occurs via recombination of the electrons, injected in ZnO nanoparticles, with OOF of the dyes [34,36]:

$$D^{\bullet+} + ZnO(e^-_{CB}) \rightarrow S_0 + ZnO \quad (20)$$

Gopidas and Kamat [34] showed that only small fraction (about 10%) of OOF takes part in rapid reverse reaction with electrons of the conduction band of colloidal semiconductor particles in the first microseconds after complete decay of the excitatory light pulse. Major part of the injected electrons remain stabilized in surface traps of a semiconductor for several milliseconds, recombining slowly with the OOF of the sensitizers.

The nature of the intermediates of pulse photolysis do not change at the addition of the monomer to the system. In Table 5 data are shown on the effect of BMA on the life-time of the intermediates of TCTIF photolysis both in the presence and in the absence of ZnO nanoparticles. At the absence of ZnO nanoparticles, monomer addition does not virtually influence on the life-time of triplet-excited dyes, but an increase in the life-time of ORF and a decrease in the life-time of OOF is observed. Analysis of these results led us to the conclusion that such behaviour of the system is connected with consumption of the OOF in the reaction with 2-propanol, leading to the formation of 1-hydroxymethylethyl radicals capable of initiating BMA polymerization chain:

$$D^{\bullet+} + (CH_3)_2CHOH \rightarrow S_0 + (CH_3)_2C^{\bullet}OH + H^+ \quad (21)$$

$$(CH_3)C^{\bullet}OH + M \rightarrow (CH_3)_2CO + HM^{\bullet} \quad (22)$$

Thus, OOF is essentially the form of the dyes responsible for the initiation of BMA polymerization.

In solutions containing ZnO nanoparticles in the presence of the monomer, substantial increase in OOF life-time is observed (see Table 5). This may be explained apparently by the appearance of a channel of the consumption of the electrons, injected into the conduction band of ZnO (*processes* 4 *and* 5) which inhibits their recombination with OOF of the dyes (*reaction* 20).

3.7. Schemes for mechanisms of photoinitiation of BMA polymerization in the presence of semiconductor nanoparticles

In Fig. 7 we represented the energy diagram of the photopolymerization system, consisting of semiconductor nanoparticles (by the example of ZnO), sensitizer (TCTIF), BMA and 2-propanol. This diagram let us discuss two schemes for the photoinitiation of BMA polymerization: (a) at the absorption of the 310–370 nm light by ZnO nanoparticles and (b) at photoexcitation of dye molecules by the light with λ > 460 nm. Analogous diagrams can be plotted for other photopolymerization compositions studied.

In accordance with the scheme (a) upon the photoexcitation of semiconductor an electron and a hole are generated in conduction and valence bands correspondingly (*process* 1), which then initiate redox-transformations of the molecules adsorbed on the surface of semiconductor nanoparticles. Holes, photogenerated in CdS, ZnO and Fe_2O_3 valence bands, oxidize 2-propanol (*reaction* 2) leading to the formation of 1-hydroxymethylethyl radicals, which, in turn, react with the monomer molecules and initiate thereby polymerization chains (*reaction* 22). In case of the smallest CdS particles studied (2.5 nm) direct BMA photoreduction by conduction band electrons takes place (*reaction* 7). In the presence of CdS nanoparticles of greater size, as well as ZnO and Fe_2O_3 nanoparticles, the interaction of conduction band electrons with protons occurs leading to atomic hydrogen formation (*reaction* 4). The later attach to monomer molecules (*reaction* 5) forming $HM^{\bullet}$ radical capable of initiation of polymerization. Thus, though direct electron transfer from the conduction band of these nanoparticles to BMA molecules is impossible, nevertheless both photogenerated electrons and holes induce the formation of two radicals, initiating BMA polymerization in the bulk of a solution:

$$HM^{\bullet} + nM \rightarrow HM_{n+1}^{\bullet} \quad (23)$$

$$RO^{\bullet} + nM \rightarrow ROM_n^{\bullet} \quad (24)$$

According to the scheme (a) dye molecules absorb the light with λ > 460 nm and are thereby excited to the first singlet and triplet states. Deactivation of the excited states of the dyes occurs via nonradiative processes (*summarized in step* 12), self-quenching at the interaction with the dye molecules in the ground state (*reaction* 13), bimolecular transformation of triplet-excited molecules resulting in the formation of ion-radicals of the dyes (ORF and OOF) (*reaction* 15) and, in the presence of ZnO nanoparticles, via the processes of

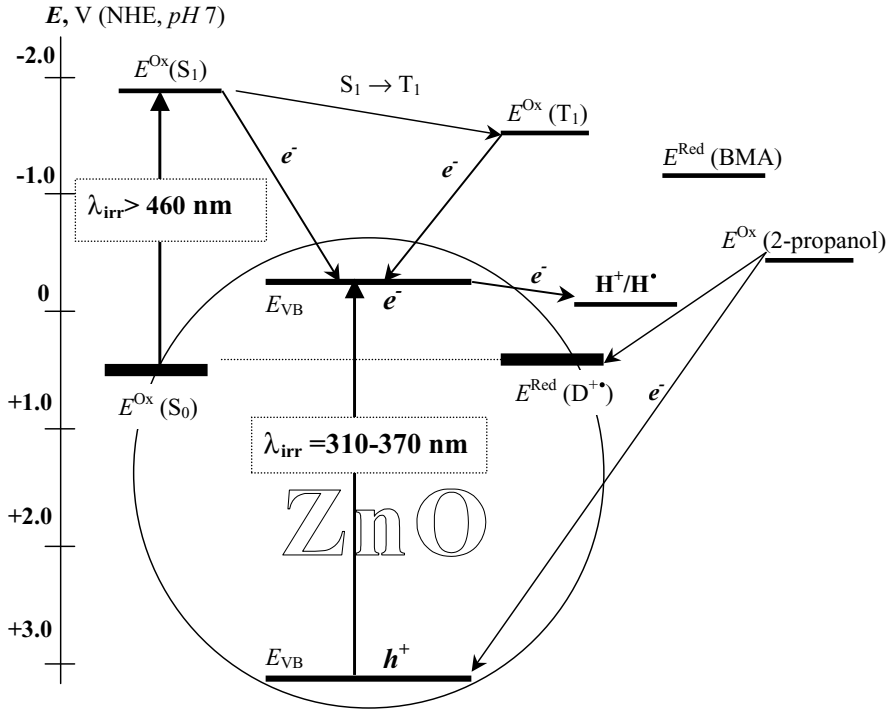

Fig. 7. Energy diagram for the photopolymerization system consisting of buthylmethacrylate (BMA), 2-propanol, ZnO nanoparticles and sensitizer – tetrachlorotetraiodofluorescein (S_0: ground state of the dye, S_1: first singlet-excited state, T_1: first triplet-excited state of the dye, E_{CB}: conduction band potential of ZnO nanoparticles, E_{VB}: valence band potential of ZnO nanoparticles). *Notes*: E^{ox} (2-propanol) = −0.22 V (NHE) [26].

electron transfer from the dyes in singlet- and triplet-excited states to the conduction band of a semiconductor (*reactions* 16 *and* 17). Electrons, localized in the traps below the bottom of the conduction band of a semiconductor, decay comparatively slowly, during hundreds of microsecond, via recombination with OOF of the dyes [12] (*reaction* 20). Monomer inhibits this process to a considerable degree due to the bounding of atomic hydrogen forming in the reaction (4) with BMA molecules (*reaction* 5). The principal process determining the life-time of OOF in the presence of the monomer is apparently a reaction between OOF of the dyes and 2-propanol molecules (*reaction* 21). Efficiency of this reaction is expected to increase in the presence of BMA owing to the consumption of 1-hydroxymethylethyl radicals in the reaction with the monomer molecules (*reaction* 22).

Chain termination occurs evidently in the bulk of a solution at the recombination of growing macroradicals and, partially, with the participation of HM• radicals accumulating in adsorption layer of semiconductor nanoparticles (*reaction* 9). The last assumption is confirmed by rather high values of the reaction orders of the monomer concentration as compared with theoretically predicted values.

4. Conclusions

It was shown in the present paper that colloidal nanoparticles of cadmium sulfide, as well as zinc and iron(III) oxides have high photocatalytic activity in free radical buthylmethacrylate polymerization in 2-propanol. Kinetic regularities of this process were studied. It was found that the specific photopolymerization rate depends on the average diameter of CdS nanoparticles. This phenomenon was explained in terms of the theory of quantum confinement effects in ultrasmall semiconductor crystals.

The possibility of the sensitization of ZnO nanoparticles to the visible light by fluorescein and some of its halogenated derivatived was established. It was found that in the presence of coupled photoinitiator consisting of ZnO nanoparticles and a sensitizer, the rate of buthylmethacrylate photopolymerization decreases in the following consequence: fluorescein > tetrachlorofluorescein > tetrabromofluorescein > tetraiodofluorescein > tetrachlorotetraiodofluorescein—symbately with a decrease in the energy of the singlet- and triplet-excited states of these dyes. Such dependence corresponds to the theory of photoinduced electron transfer with the participation of photoexcited dye molecules and a semiconductor and indicates on determining role of the rate of electron transfer from excited sensitizers to the conduction band of ZnO nanoparticles in the initiation of buthylmethacrylate polymerization in the systems studied.

References

[1] C. Decker, Opt. Memory Neural Networks 10 (2001) 125.
[2] B.M. Monroe, G.C. Weed, Chem. Rev. 93 (1993) 435.

[3] J.C. Kuriacose, M.C. Markham, J. Phys. Chem. 65 (1961) 2232.
[4] B. Kraeutler, H. Reiche, A.J. Bard, J. Polym. Sci., Polym. Lett. Ed. 17 (1979) 535.
[5] B.L. Funt, S.-R. Tan, J. Polym. Sci., Polym. Chem. Ed. 22 (1984) 605.
[6] P.V. Kamat, R. Basheer, M.A. Fox, Macromolecules 18 (1985) 1366.
[7] P.V. Kamat, R.V. Todesco, J. Polym. Sci. A-Polym. Chem. 25 (1987) 1035.
[8] A.J. Hoffman, H. Yee, G. Mills, M.R. Hoffmann, J. Phys. Chem. 96 (1992) 5540.
[9] A.J. Hoffman, G. Mills, H. Yee, M.R. Hoffmann, J. Phys. Chem. 96 (1992) 5546.
[10] Z.-Y. Huang, T. Barber, G. Mills, M.-B. Morris, J. Phys. Chem. 98 (1994) 12746.
[11] A. Henglein, Ber. Bunsenges. Phys. Chem. 101 (1997) 1562.
[12] A.P. Alivisatos, J. Phys. Chem. 100 (1996) 13226.
[13] T. Hirai, T. Watanabe, I. Komasawa, J. Phys. Chem. B 104 (2000) 8962.
[14] N.P. Gaponik, D.V. Sviridov, Ber. Bunsenges. Phys. Chem. 101 (1997) 1657.
[15] J. Calvert, J. Pitts Photochemistry, Wiley, New York, 1967.
[16] D.W. Bahmemann, Isr. J. Chem. 33 (1993) 115.
[17] E.M. Wong, P.G. Hörtz, G.J. Liang, B.-M. Shi, G.J. Meyer, P.C. Searson, Langmuir 17 (2001) 8362.
[18] N.M. Dimitrijevič, D. Savič, Î.I. Micič, A.J. Nozik, J. Phys. Chem. 88 (1984) 4278.
[19] J.K. Leland, A.J. Bard, J. Phys. Chem. 91 (1987) 5076.
[20] B.C. Faust, M.R. Hoffmann, D.W. Bahnemann, J. Phys. Chem. 93 (1989) 6371.
[21] F.A. Cotton, F. Wilkinson, Advanced Inorganic Chemistry, Wiley, New York, 1967.
[22] T. Vossmeyer, L. Katsikas, M. Giersig, I.G. Popovic, K. Diesner, A. Chemseddine, A. Eychmueller, H. Weller, J. Phys. Chem. 98 (1994) 7665.
[23] C. Liu, A.J. Bard, J. Phys. Chem. 93 (1989) 3232.
[24] B. Enright, D. FitzMaurice, J. Phys. Chem. 100 (1996) 1027.
[25] A. Wood, M. Giersig, P. Mulvaney, J. Phys. Chem. B 105 (2001) 8810.
[26] M. Clark, Oxidation–Reduction Potentials of Organic Systems, Baltimor, 1960.
[27] P.V. Kamat, B. Patrick, J. Phys. Chem. 96 (1992) 6829.
[28] B. Patric, P.V. Kamat, J. Phys. Chem. 96 (1992) 1423.
[29] J.-E. Moser, M. Wolf, F. Lenzmann, M. Grätzel, Z. Phys. Chem. 212 (1999) 85.
[30] T. Sakata, K. Hashimoto, M. Hiramoto, J. Phys. Chem. 94 (1990) 3040.
[31] J. Chrysochoos, J. Ovadia, L.I. Groβweiner, J. Phys. Chem. 71 (1967) 1629.
[32] L.A. Flamingi, J. Phys. Chem. 96 (1992) 3331.
[33] C. Lambert, T. Sarna, T.G. Truscott, J. Chem. Soc., Faraday Trans. 86 (1990) 3879.
[34] K.R. Gopidas, P.V. Kamat, J. Phys. Chem. 93 (1989) 6428.
[35] T. Ohno, S. Kato, M. Koizumi, Bull. Chem. Soc. Jpn. 39 (1966) 232.
[36] G. Benkoe, M. Hilgendorff, A.P. Yartzev, V. Sundström, J. Phys. Chem. B 105 (2001) 967.